Catalytic cascade vapor-phase hydrotreating of plastic waste into fuels and its sustainability assessment

Jia Wang [a, b], Jianchun Jiang [a, b], Xinyue Dong [c], Yiyun Zhang [b], Xiangzhou Yuan [d], Xianzhi Meng [e], Guowu Zhan [f], Lei Wang [c*], Yanqin Wang [g], Arthur J. Ragauskas [e, h, i]*

[a] *Jiangsu co-Innovation Center for Efficient Processing and Utilization of Forest Resources, College of Chemical Engineering, Nanjing Forestry University, Longpan Road 159, Nanjing 210037, China*

[b] *Institute of Chemical Industry of Forest Products, Chinese Academy of Forestry (CAF), No. 16, Suojin Five Village, Nanjing 210042, China*

[c] *Key Laboratory of Coastal Environment and Resources of Zhejiang Province , School of Engineering, Westlake University, Hangzhou 310024, Zhejiang Province, China*

[d] *Korea Biochar Research Center, APRU Sustainable Waste Management & Division of Environmental Science and Ecological Engineering, Korea University, Seoul, 02841, Republic of Korea*

[e] *Department of Chemical and Biomolecular Engineering, The University of Tennessee, Knoxville, TN 37996, USA*

[f] *College of Chemical Engineering, Huaqiao University, 668 Jimei Avenue, Xiamen, Fujian, 361021, P. R. China*

[g] *Key Laboratory for Advanced Materials and Joint International Research Laboratory of Precision Chemistry and Molecular Engineering, Feringa Nobel Prize Scientist Joint Research Center, Research Institute of Industrial Catalysis, School of Chemistry and Molecular Engineering, East China University of Science and Technology, Shanghai 200237, China*

[h] *Center for Renewable Carbon, Department of Forestry, Wildlife and Fisheries, The University of Tennessee, Knoxville, TN 37996, USA*

[i] *Joint Institute of Biological Sciences, Biosciences Division, Oak Ridge National Laboratory, Oak Ridge, TN 37831, USA*

* Corresponding author.

E-mail address: jiangjc@caf.ac.cn; wang_lei@westlake.edu.cn

Catalyst preparation

$Ni/NiAl_2O_4$ spinel was synthesized by a co-precipitation method at a Ni/Al mole ratio of 1:2. Typically, 40 mmol nickel (Ni) nitrate hexahydrate and 80 mmol aluminum (Al) nitrate nonahydrate were dissolved in 200 mL ultra-pure water (18.2 mΩ) under vigorous stirring at room temperature. Aqueous ammonia was added dropwise to the above solution until the pH value reached 8. After stirring for another one hour, the formed precipitate was kept for overnight aging at room temperature. Then, the precipitates were filtered and washed by deionized water until the pH of filtrate reached 7. Finally, the precipitates were dried for 12 h at 100 ºC, followed by the calcination for 8 h at 800 ºC under pure N_2 atmosphere.

Catalyst characterization

The X-ray diffraction (XRD) patterns of catalysts were determined by a Bruker D8 Advance using CuKα radiation, with the scanning range of 2θ varying from 5º to 90º (10^o min^{-1}). The N_2 adsorption/desorption was conducted to investigate the porosity and surface area via a Micromeritics ASAP 2460 instrument. The acidic properties of catalysts were characterized by ammonia temperature-programmed desorption (NH_3-TPD) by a Micromeritics Autochem II 2920. The catalysts were pretreated (100 mg for each run) under He at a temperature of 450 °C for 1 h and then were saturated with 10% NH_3/He (50 mL/min) at 100 °C for 1 h. Finally, the catalysts were purged with Ar (150 °C, 1 h), and the TPD was recorded from 50 to 800 ºC with a 10 °C/min heating rate.

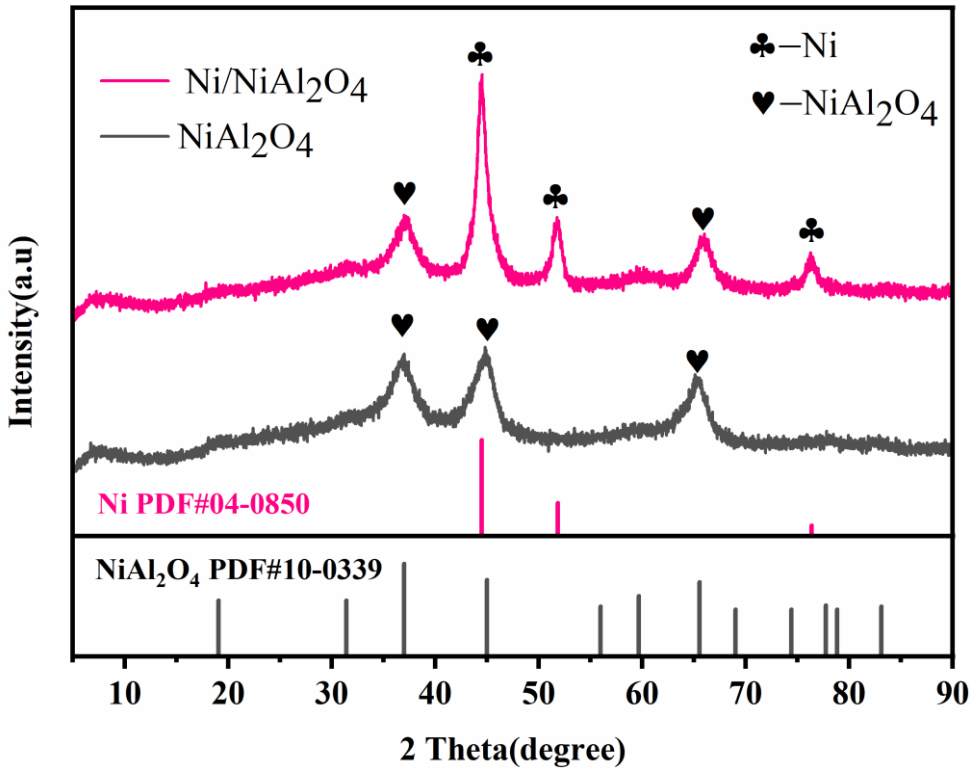

Fig. S1. XRD patterns of $NiAl_2O_4$ and $Ni/NiAl_2O_4$ (reduced $NiAl_2O_4$) catalysts.

The phase identification and crystallinity of the calcined and reduced catalysts were investigated by XRD (Fig. S1). The $NiAl_2O_4$ catalyst showed the characteristic diffraction peaks at 2θ = 37.0°, 45.0°, and 65.5° corresponding to the (3 1 1), (4 0 0), and (4 4 0) planes of $NiAl_2O_4$ (PDF#10-0339), respectively. Noteworthy, two diffraction peaks were observed at 2θ = 44.5°, 51.8°, and 76.4°for the reduced $Ni/NiAl_2O_4$, which belonged to the (111), (200), and (220) planes of the metallic Ni phase, respectively.

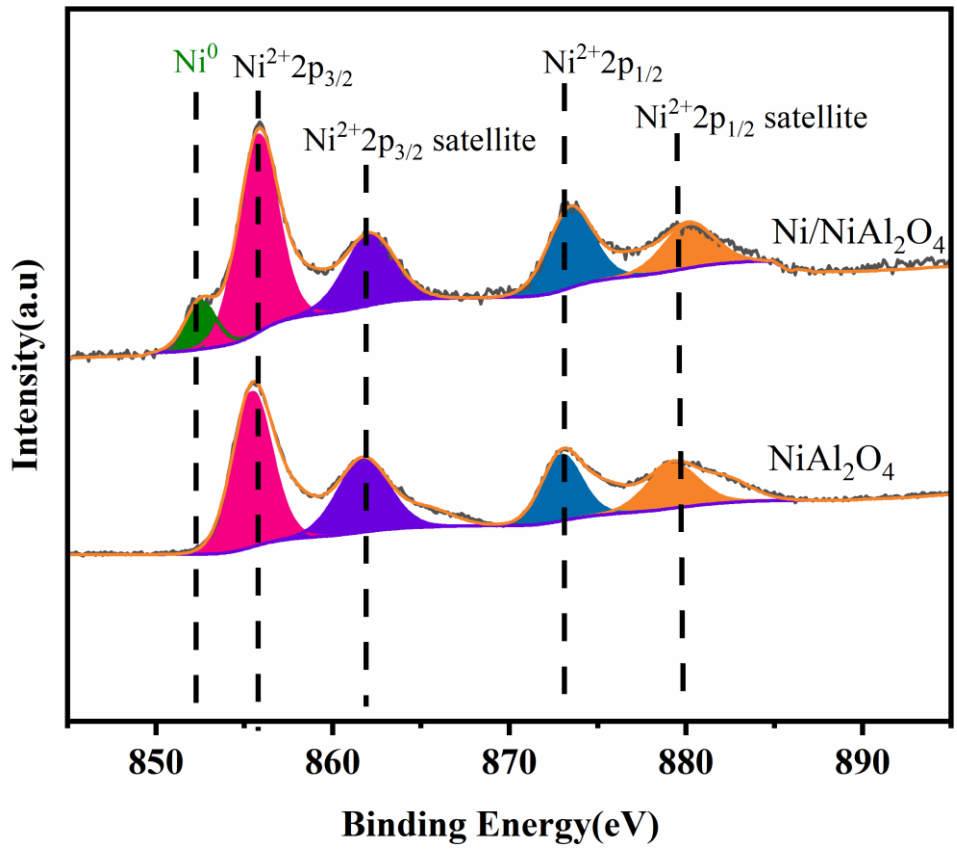

Fig. S2. XPS for calcined catalysts and reduced catalysts

The XPS spectrum of calcined and reduced catalysts were shown in Fig. S2. As illustrated, the high-resolution XPS of the Ni 2p peak spectrum can be deconvoluted into four peaks, including $Ni^{2+}2p_{3/2}$ (855.7 eV), $Ni^{2+}2p_{3/2}$ satellite (862.7 eV), $Ni^{2+}2p_{1/2}$ (873 eV) and $Ni^{2+}2p_{1/2}$ satellite (880 eV). The presence of Ni^0 species is observed at ~ 852.6 eV for the reduced catalyst, which is agreed well with XRD results.

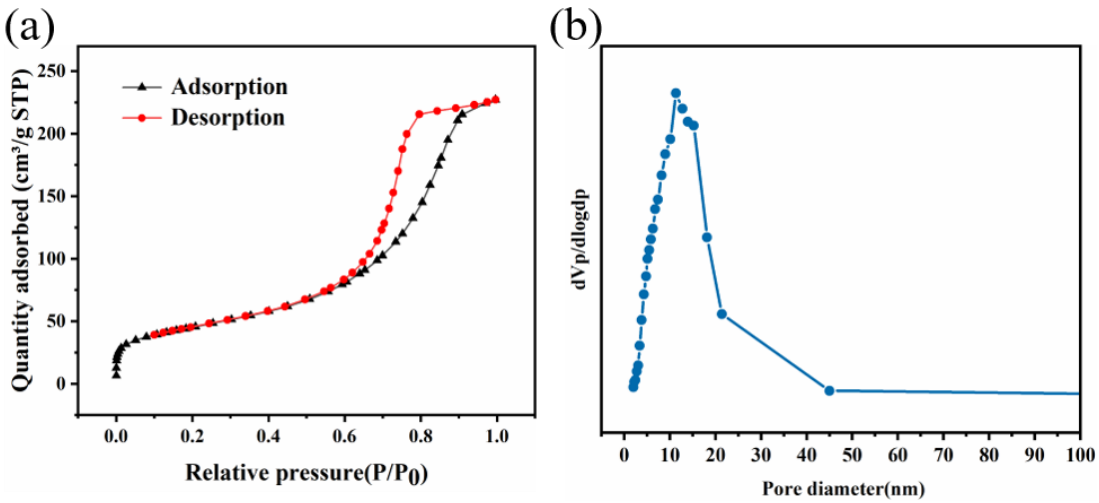

Fig. S3. N_2-adsorption-desorption profiles of $Ni/NiAl_2O_4$.

The physical properties of the catalysts were investigated by N_2 adsorption-desorption and the results are summarized in Table S1 and Fig. S3. The N_2 adsorption and desorption isotherms is a type IV for $Ni/NiAl_2O_4$ catalysts, with an H_2 type hysteresis loop at P/P_0 = 0.6 to 0.9, indicating the presence of mesopores structure. The surface area and total pore volume of the $NiAl_2O_4$ catalyst are 159 m^2/g and 0.35 cm^3/g, respectively. The average pore size of $Ni/NiAl_2O_4$ is ~8nm.

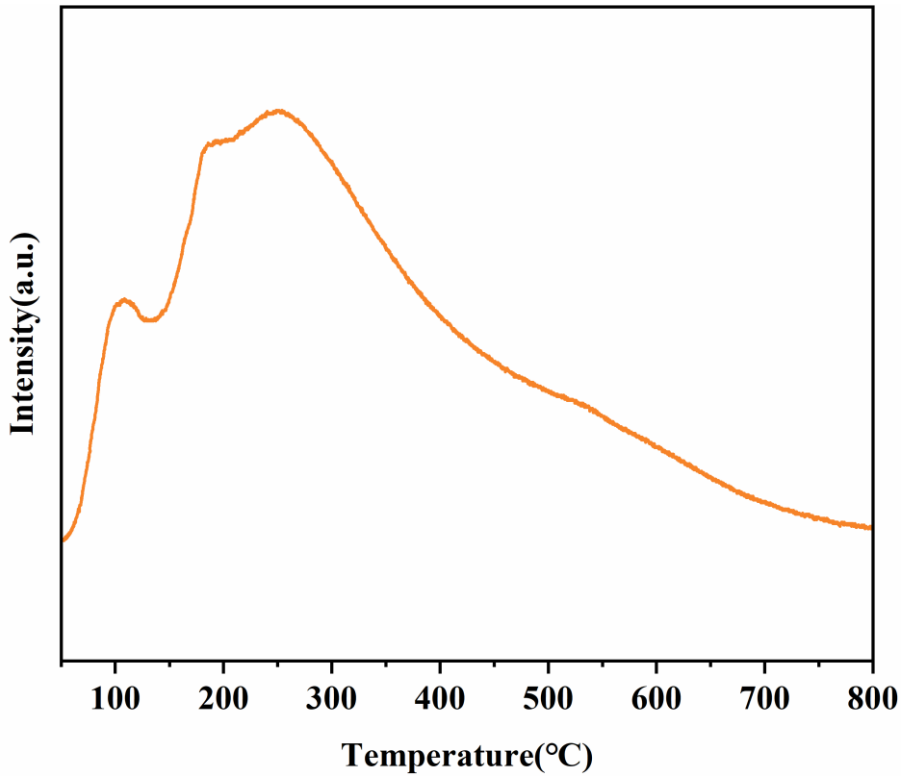

Fig. S4. NH_3-TPD of $Ni/NiAl_2O_4$ catalysts.

The acid characteristics of the $Ni/NiAl_2O_4$ catalysts were evaluated by NH_3-TPD, and the results are shown in Fig. S4 and Table S1. The $NiAl_2O_4$ catalysts exhibited two ammonia desorption peak at 110 ℃ and 250 ℃, corresponding to weak (0.016 mmol/g, Table 1) and medium strong acid sites (0.167 mmol/g, Table 1), respectively. Moreover, the acid sites for per surface area (i.e., Total acid sites concentration expressed per 1 m^2, Table S1) was calculated, and the T_{acid}/S_{BET} is 1.15 μmol/m^2.

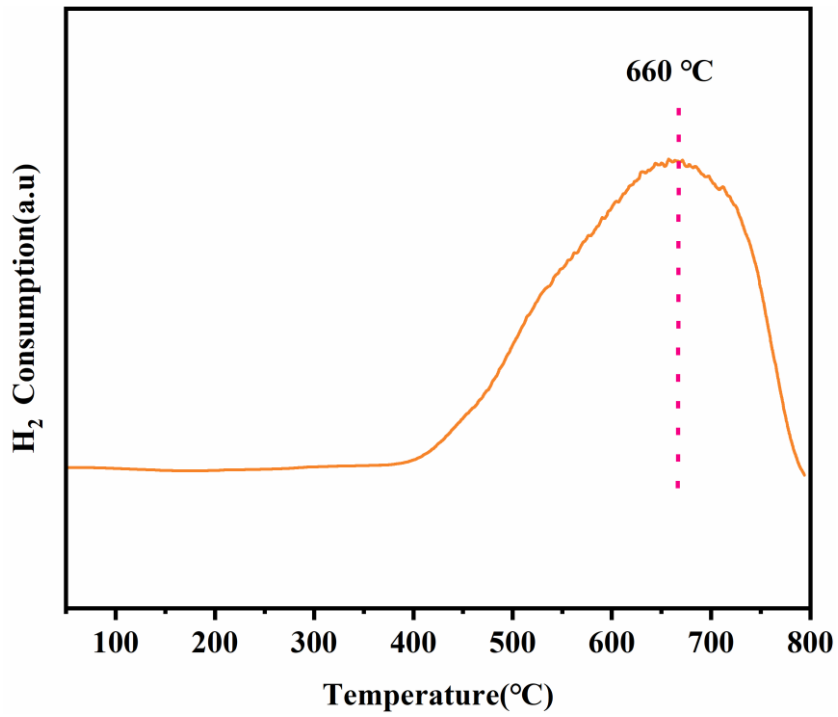

Fig. S5. H_2-TPR of $Ni/NiAl_2O_4$ catalysts

The H_2-TPR profile of the $Ni/NiAl_2O_4$ catalyst is shown in Fig. S5. The higher reduction peak around 660 °C is ascribed to the reduction of Ni^{2+} to Ni^0 in the crystal phase of $Ni/NiAl_2O_4$. The H_2 consumption was calcualated and the result is summarized in Table S1. As indicated, the $Ni/NiAl_2O_4$ has considerable reducible perfromance with a H_2 consumption of 5.87 mmol/g.

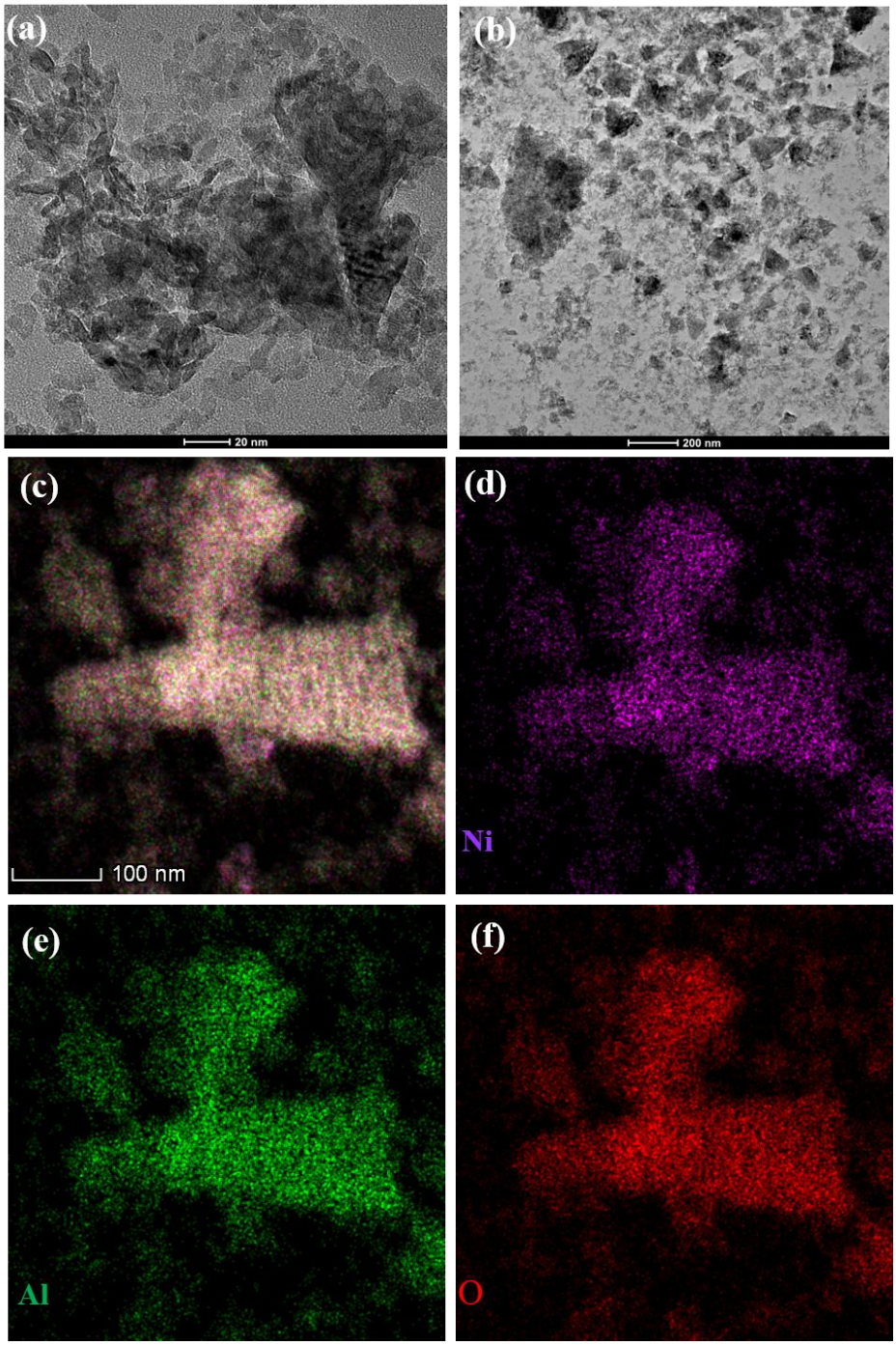

Fig. S6. TEM-EDS mapping of $Ni/NiAl_2O_4$ catalysts.

The microstructure and particle distribution of the prepared $Ni/NiAl_2O_4$ catalysts are analyzed by TEM and energy-dispersive X-ray spectroscopy (EDS) mapping, and the TEM-EDS in Fig. S6 illustrated that the distribution of Ni and Al species in $Ni/NiAl_2O_4$ was very homogeneous. Moreover, no larger particle size agglomerates were observed for $Ni/NiAl_2O_4$.

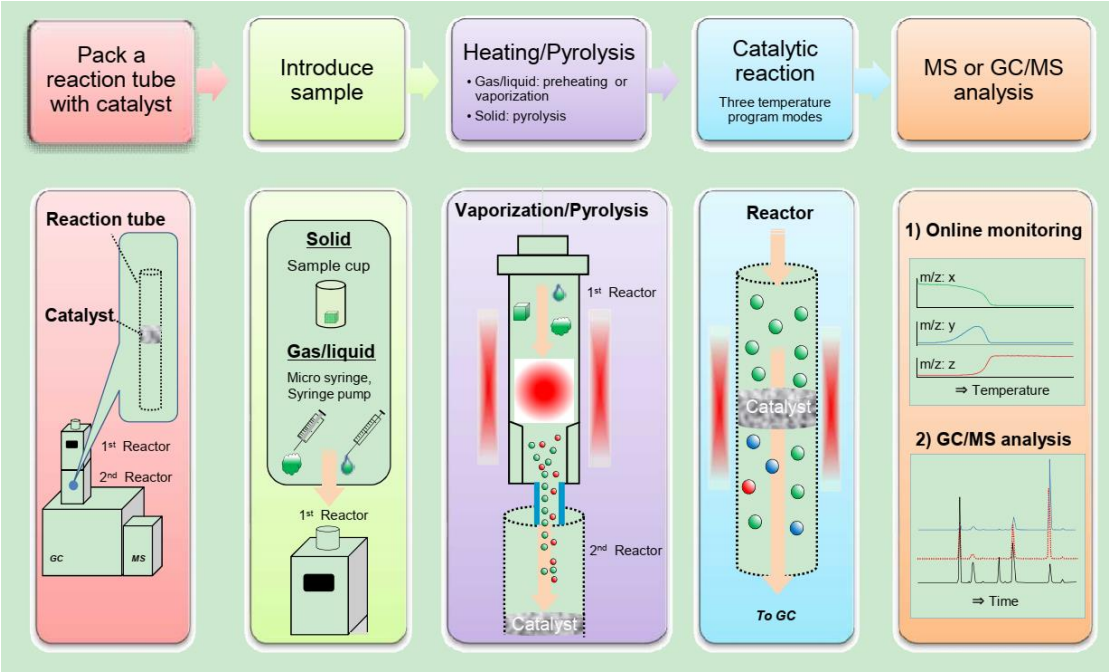

Fig. S7. Schematic diagram of the two-stage pressurized fixed-bed reactor used for the tandem hydrotreating of COVID-19-derived polymer wastes (A), and typical reaction process (B).

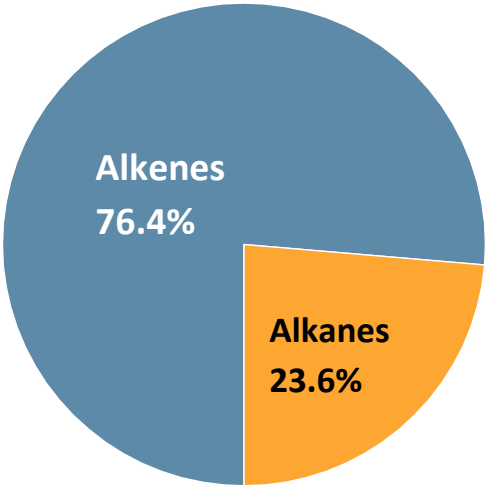

Fig. S8. Selectivity of hydrocarbons obtained from non-catalytic tandem conversion of PE bags: PE conversion = 98.7%.

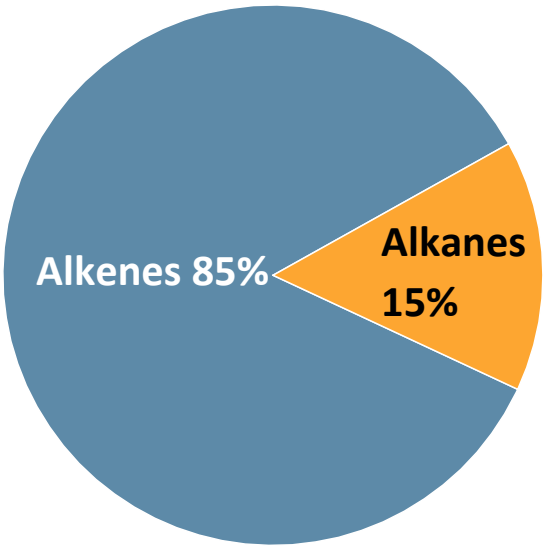

Fig. S9. Selectivity of hydrocarbons obtained from non-catalytic tandem conversion of disposable masks: Conversion = 99.1%

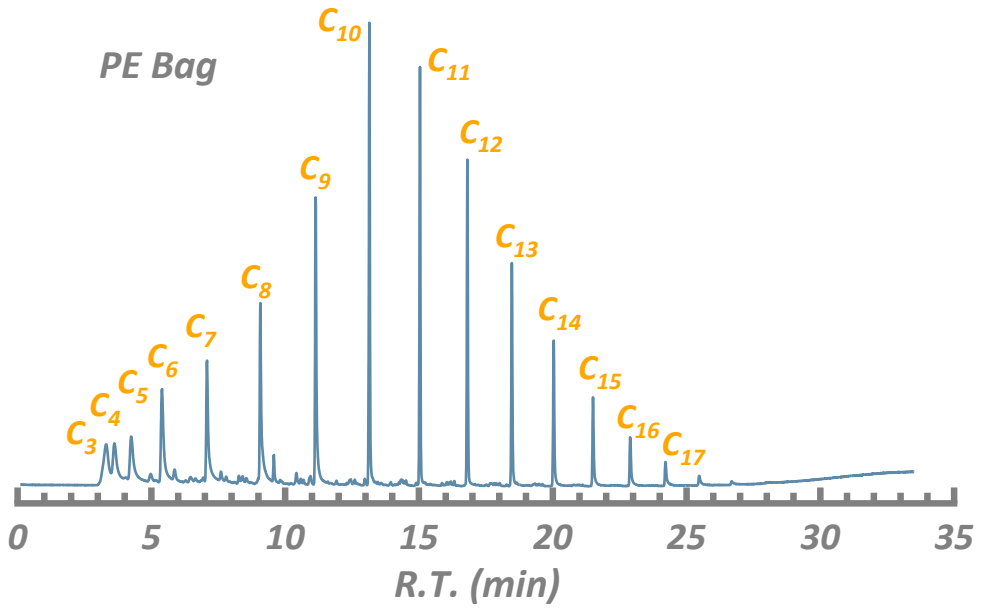

Fig. S10. TIC chromatogram of $Ni/NiAl_2O_4$ catalyzed PE bags via the catalytic tandem hydrotreating conversion process.

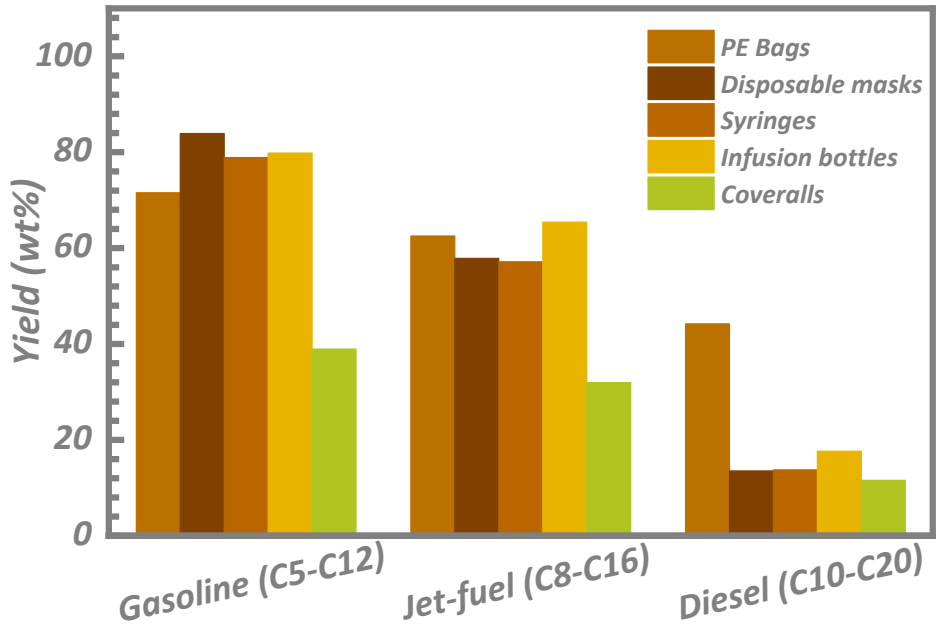

Fig. S11. Yield of fuel-range alkanes obtained from catalytic tandem conversion of polyolefins over $Ni/NiAl_2O_4$.

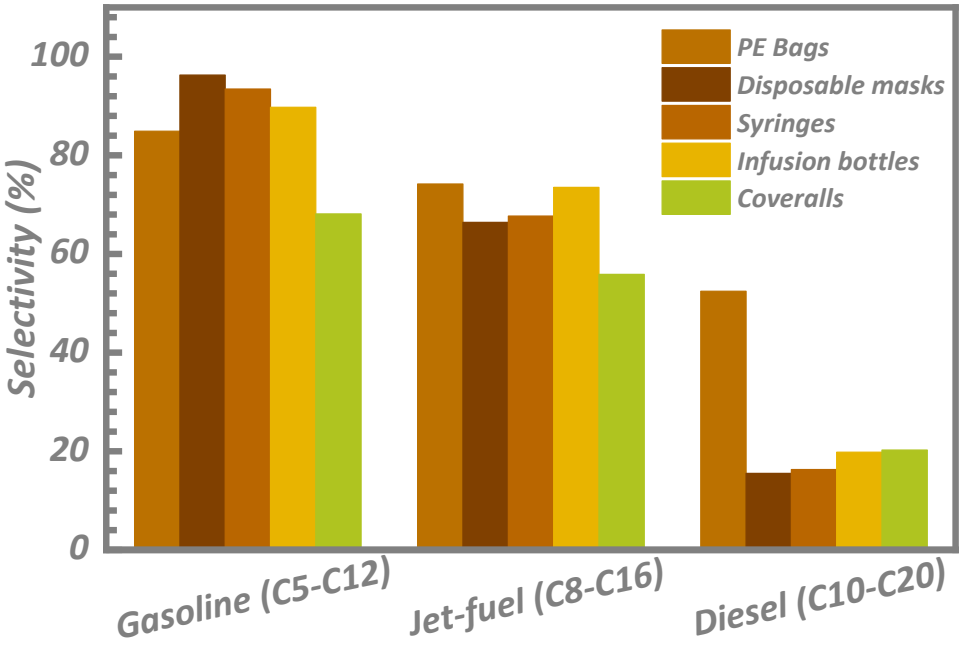

Fig. S12. Selectivity of fuel-range alkanes obtained from catalytic tandem conversion of polyolefins over $Ni/NiAl_2O_4$.

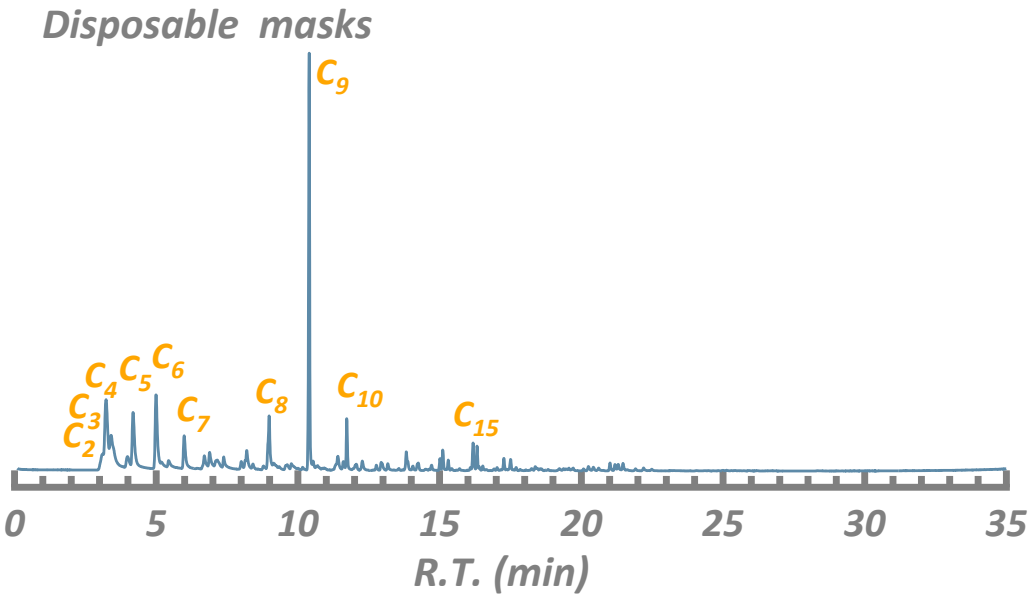

Fig. S13. TIC chromatogram of $Ni/NiAl_2O_4$ spinel catalyzed disposable masks via the tandem hydrotreating conversion process.

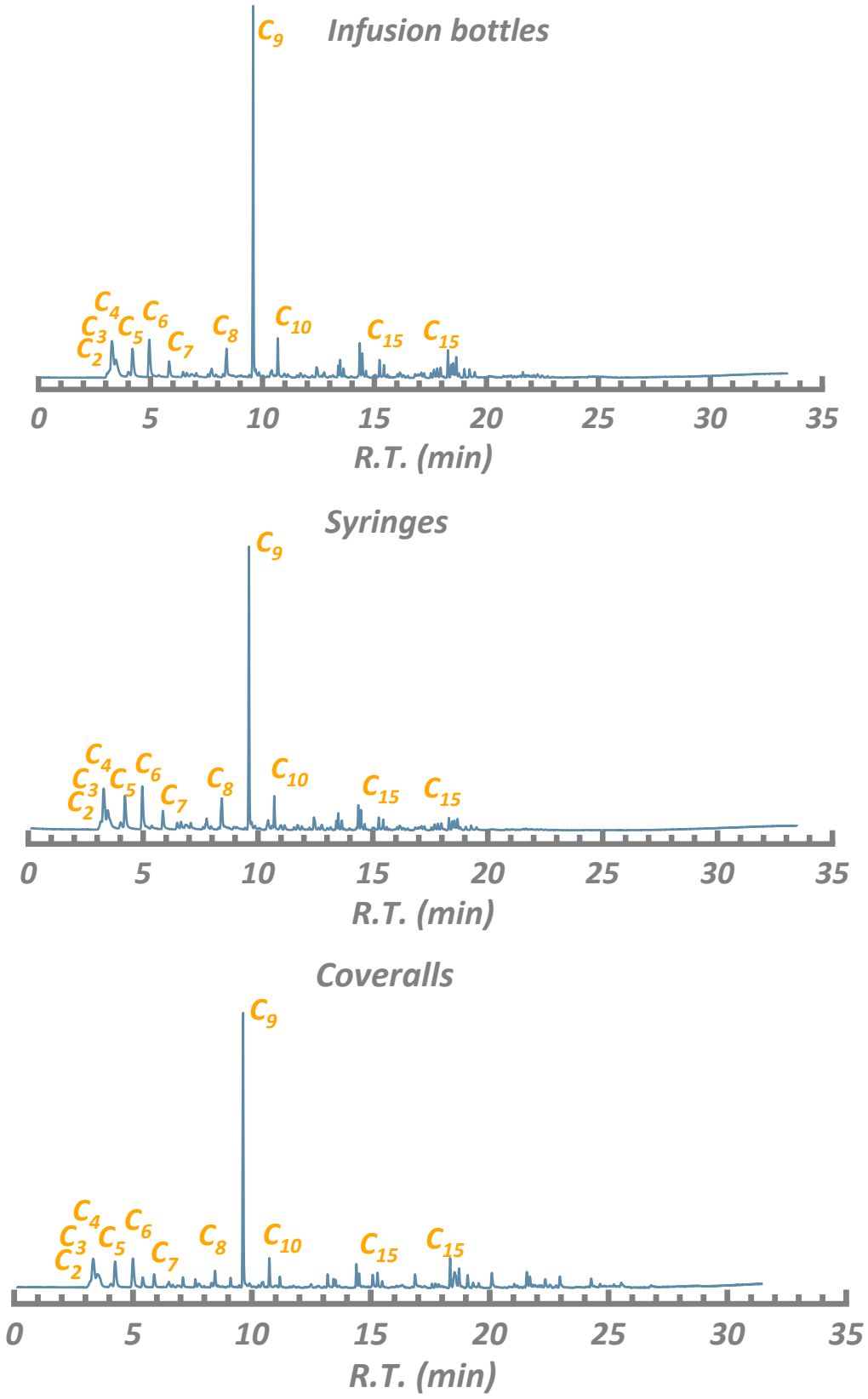

Fig. S14. TIC chromatograms of Ni/$NiAl_2O_4$ catalyzed PP-based PPE plastic wastes via the tandem hydrotreating conversion process.

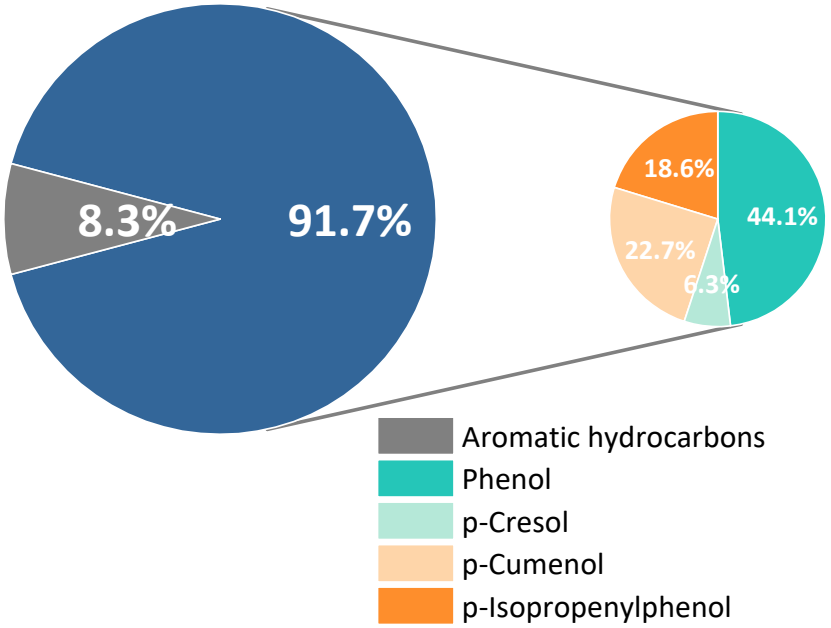

Fig. S15. Selectivity of aromatics obtained from non-catalytic tandem conversion of goggles: Conversion = 88.6%.

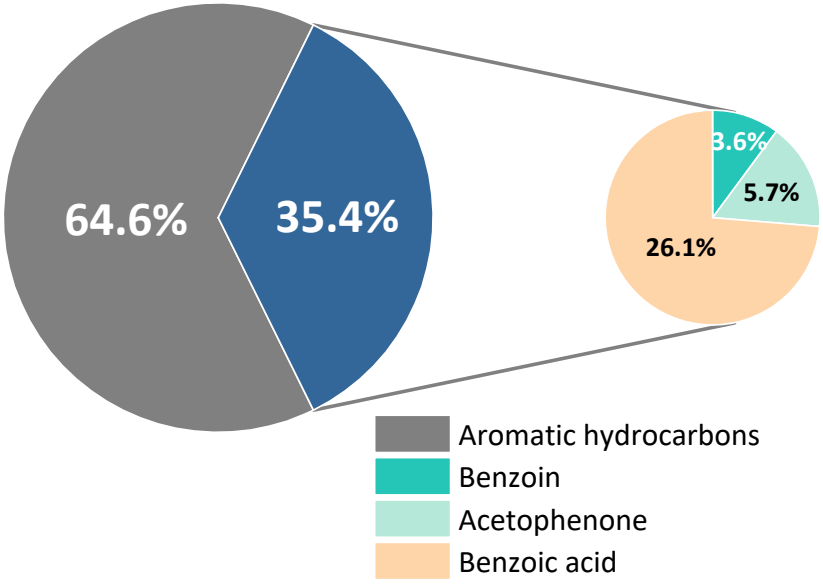

Fig. S16. Selectivity of aromatics obtained from non-catalytic tandem conversion of face shields: Conversion = 85.4%

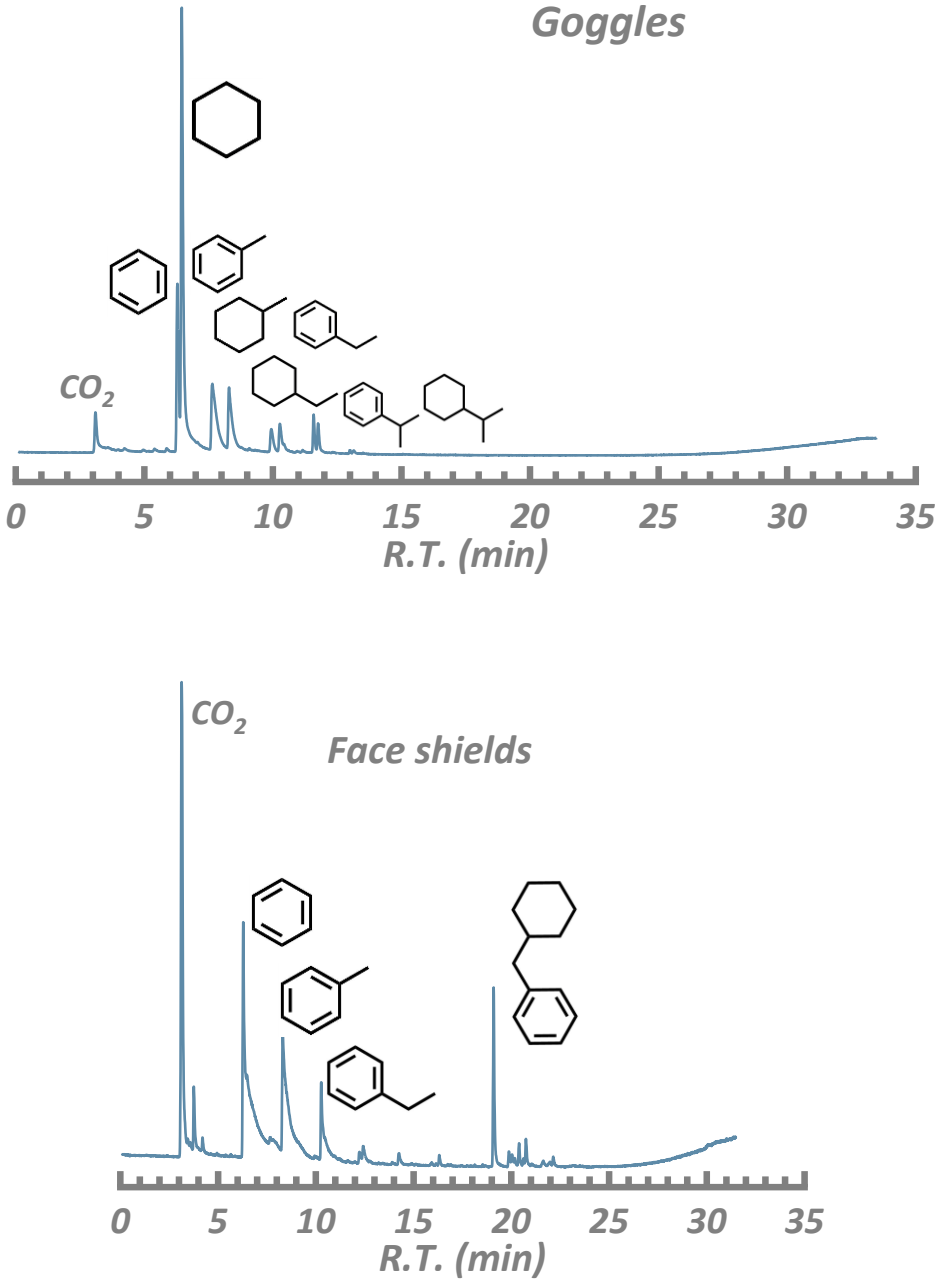

Fig. S17. TIC chromatogram of $Ni/NiAl_2O_4$ catalyzed goggles and face shields via the tandem hydrotreating conversion process.

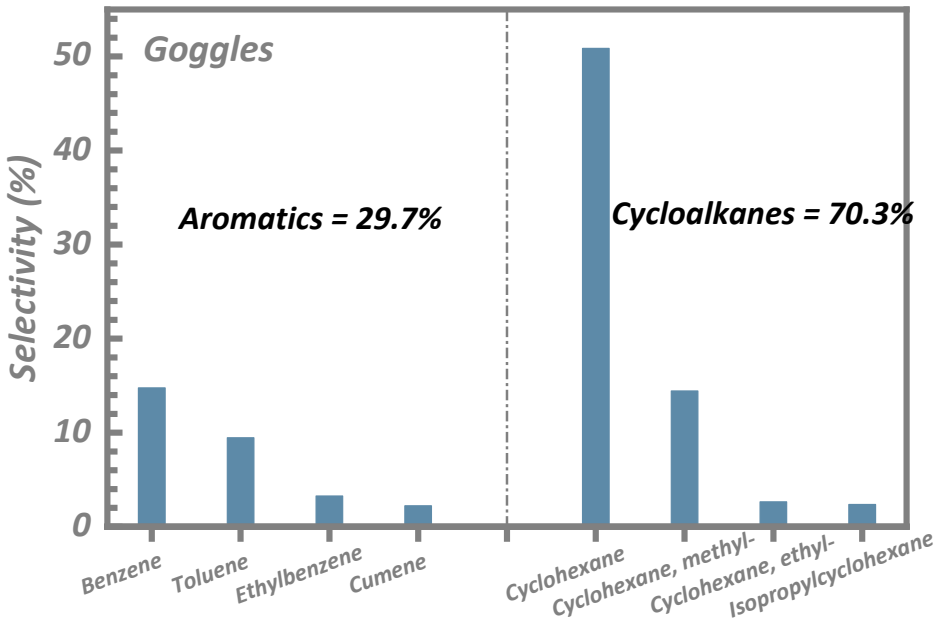

Fig. S18. Selectivity of fuel-range hydrocarbons obtained from catalytic tandem hydrotreating of goggles over $Ni/NiAl_2O_4$.

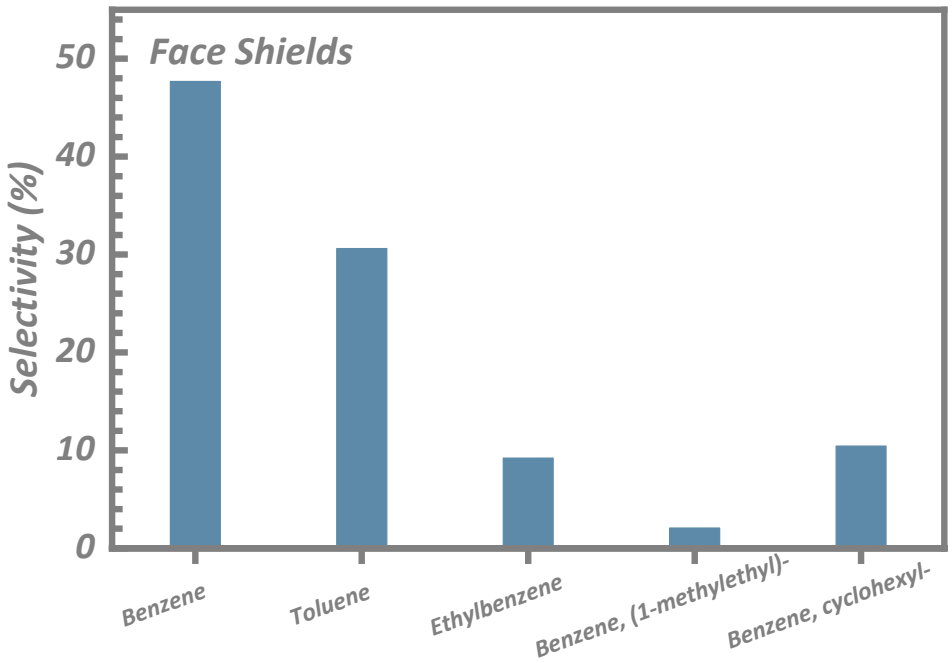

Fig. S19. Selectivity of fuel-range hydrocarbons obtained from catalytic tandem hydrotreating of face shields over $Ni/NiAl_2O_4$.

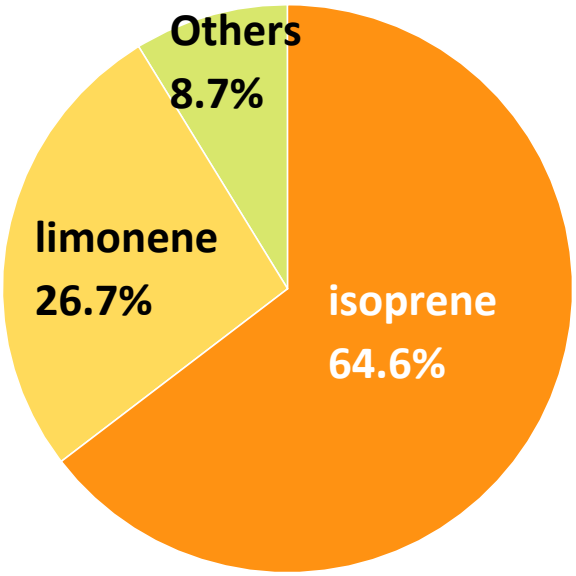

Fig. S20. Selectivity of hydrocarbons obtained from non-catalytic conversion of natural rubber glove wastes: Conversion = 93.0%.

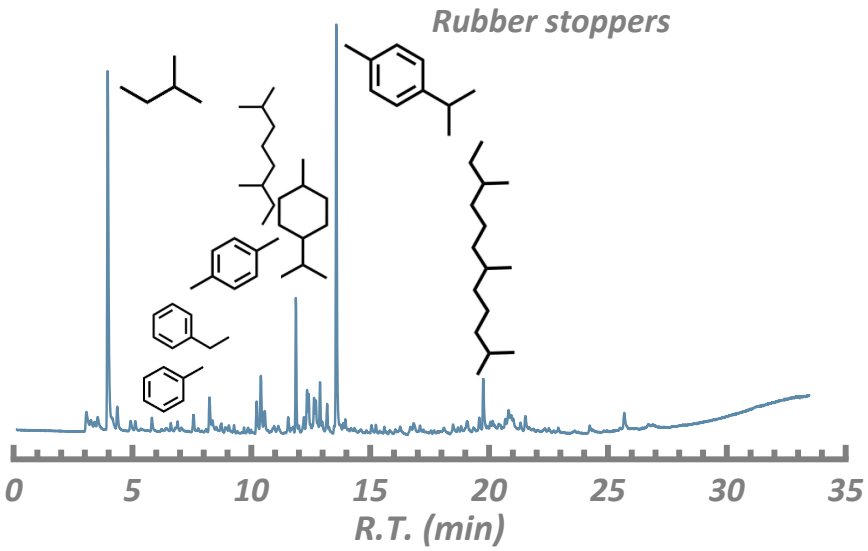

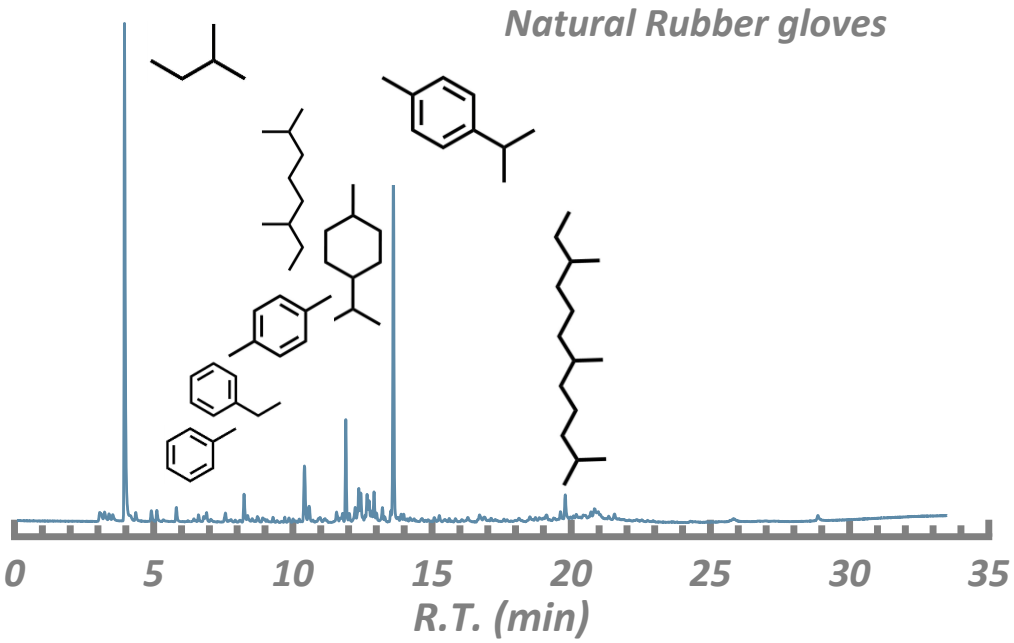

Fig. S21. TIC chromatograms of $Ni/NiAl_2O_4$ catalyzed rubbers via the tandem hydrotreating conversion process.

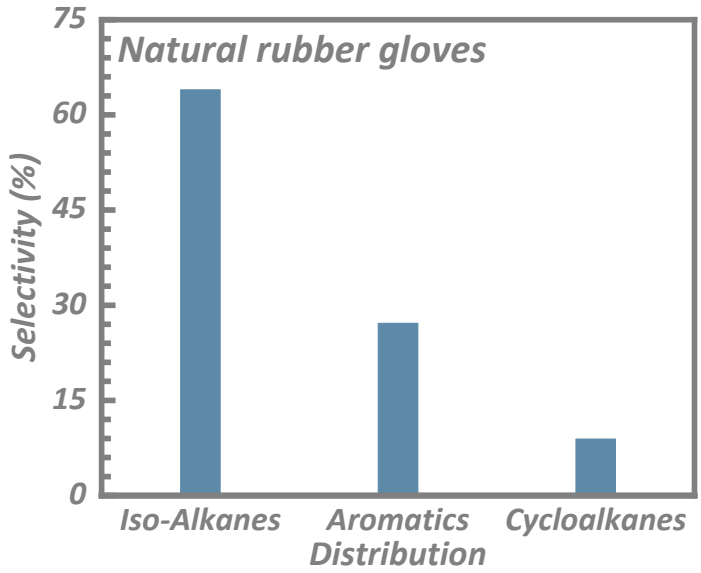

Fig. S22. Selectivity of fuel-range hydrocarbons obtained from the tandem hydrotreating conversion of natural rubber gloves over $Ni/NiAl_2O_4$.

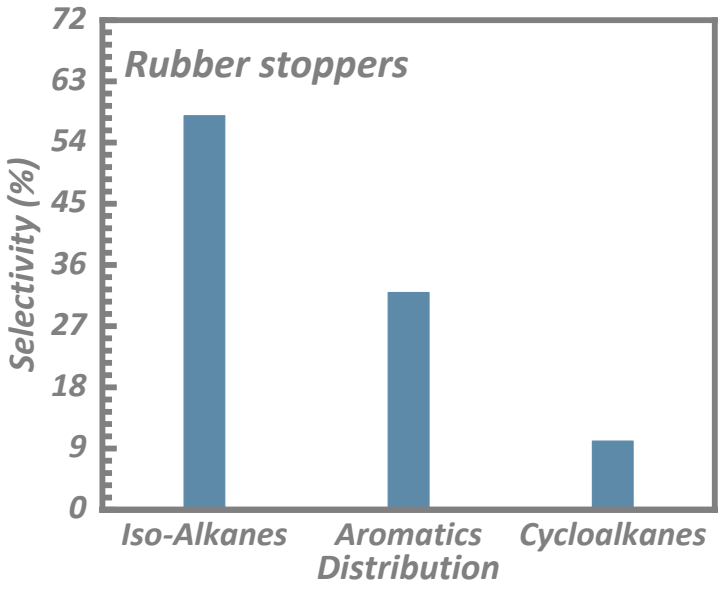

Fig. S23. Selectivity of fuel-range hydrocarbons obtained from the tandem hydrotreating conversion of rubber stoppers over $Ni/NiAl_2O_4$.

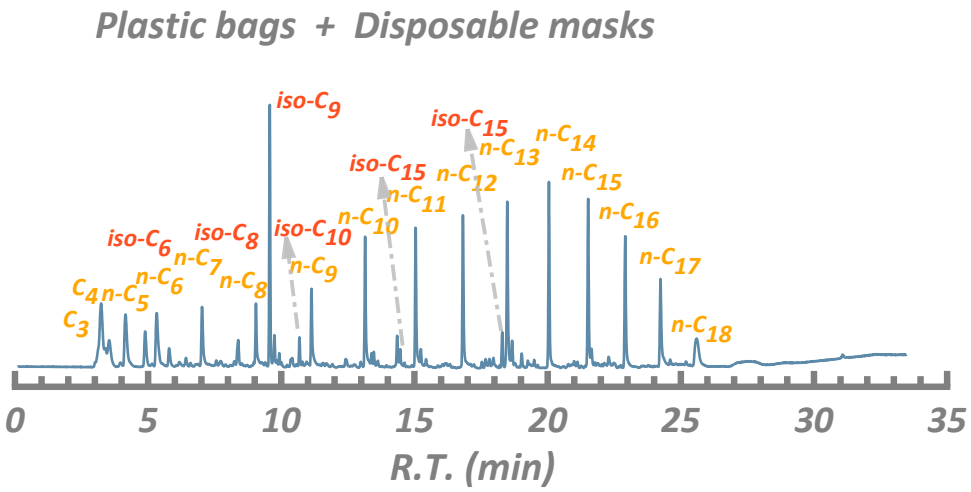

Fig. S24. TIC chromatogram of $Ni/NiAl_2O_4$ spinel catalyzed mixed PE bags and disposable masks via the tandem hydrotreating conversion process.

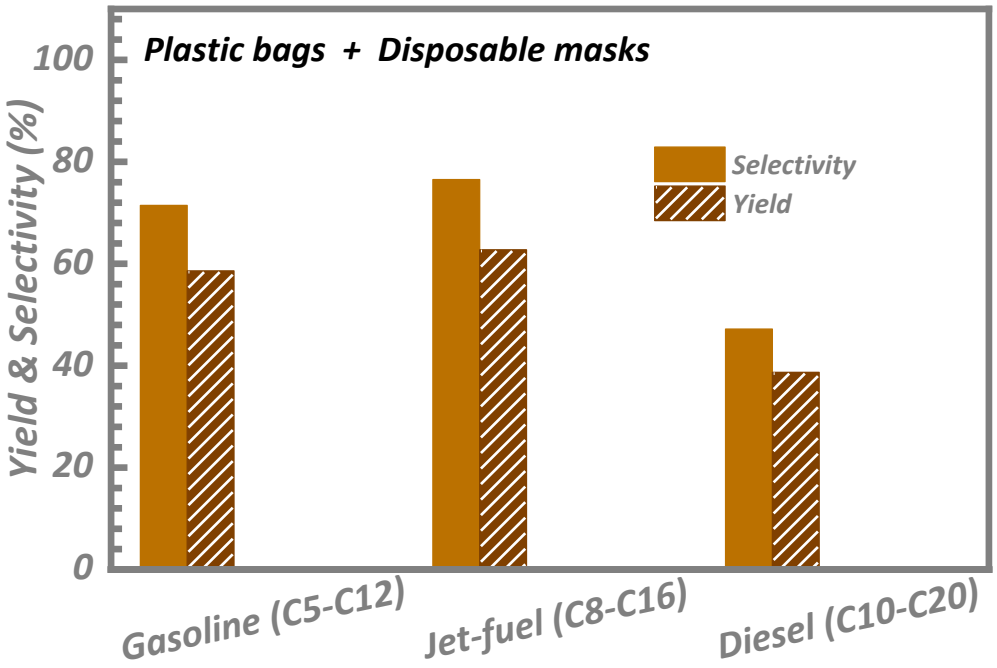

Fig. S25. Selectivity of fuel-range alkanes obtained from the tandem hydrotreating conversion of mixed PE bags and disposable masks over $Ni/NiAl_2O_4$.

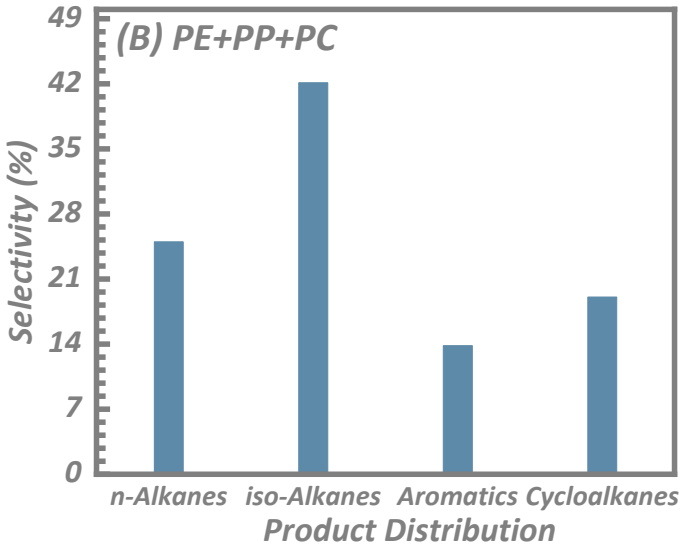

Fig. S26. Selectivity of fuel-range hydrocarbons obtained from the tandem hydrotreating conversion of mixed PE bags, disposable masks, and goggles over $Ni/NiAl_2O_4$.

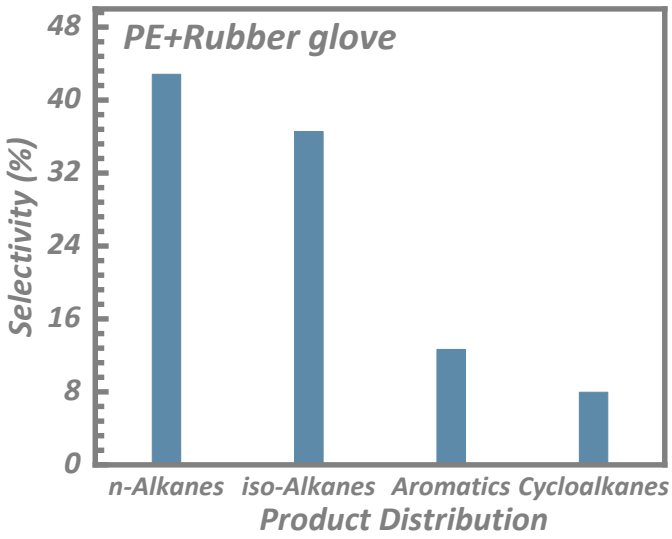

Fig. S27. Selectivity of fuel-range hydrocarbons obtained from the tandem hydrotreating conversion of mixed PE bags and natural rubber gloves over $Ni/NiAl_2O_4$.

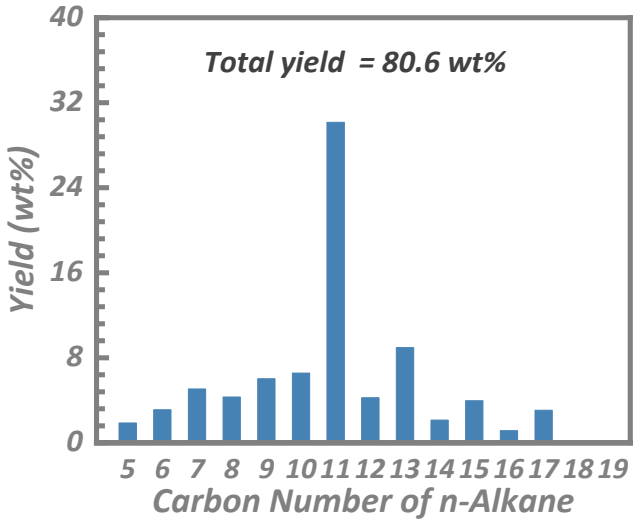

Fig. S28. Distribution in fuel-range n-alkanes obtained from the tandem hydrotreating conversion of palm kernel oil over $Ni/NiAl_2O_4$.

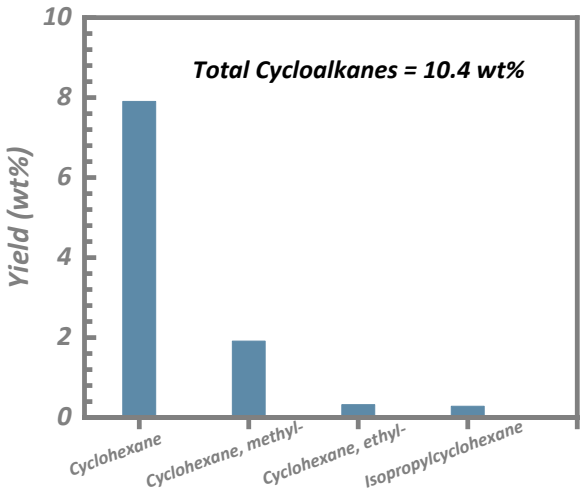

Fig. S29. Distribution in fuel-range hydrocarbons obtained from the tandem hydrotreating conversion of lignin over Ni/$NiAl_2O_4$.

Table S1. Textural properties and acidity of various catalysts.

Samples	S_{BET} [a] (m^2/g)	TV [b] (cm^3/g)	PD [c] (nm)	Acid Content ((μmol/g) [d]			T_{acid}/S_{BET} [g] ($\mu mol/m^2$)	H_2 uptake [h] (mmol/g)
				weak [e]	strong [f]	Total		
$NiAl_2O_4$	158.9	0.35	8.81	16.0	167.0	183.0	1.15	5.87

[a] Total surface area, by BET; [b] Total pore volume, calculated at p/p_0 = 0.99; [c] Adsorption average pore diameter (4V/A by BET); [d] by NH_3-TPD; [e] weak acid sites; [f] medium strong acid sites; [g] Total acid sites concentration expressed per 1 m^2; [h] by H_2-TPR.